

Phonon dispersions in niobium determined by x-ray transmission scatteringM. Holt,^{1,2} P. Czoschke,^{1,2} Hawoong Hong,¹ P. Zschack,¹ H. K. Birnbaum,¹ and T.-C. Chiang^{1,2,*}¹*Frederick Seitz Materials Research Laboratory, University of Illinois at Urbana-Champaign, 104 South Goodwin Avenue, Urbana, Illinois 61801-2902*²*Department of Physics, University of Illinois at Urbana-Champaign, 1110 West Green Street, Urbana, Illinois 61801-3080*

(Received 10 April 2002; published 16 August 2002)

Quasielastic x-ray scattering from thermally populated phonons in crystalline niobium was recorded using a charge-coupled device over a large angular range. The patterns, displayed on a logarithmic intensity scale, reveal rich features. Theoretical patterns based on a lattice dynamics calculation are generated, and a least-squares simultaneous fit of these patterns recorded at several incidence angles yields phonon dispersion relations over the entire reciprocal space. The dispersions along high-symmetry directions are generally in good accordance with available neutron scattering data.

DOI: 10.1103/PhysRevB.66.064303

PACS number(s): 78.70.Ck, 63.20.Dj

Historically, analysis of x-ray thermal diffuse scattering (TDS) is among the oldest experimental methods that deal with the dispersion of phonons in crystals. This method was first proposed by Laval¹ in 1938, but remained impractical and was almost immediately abandoned with the advent of neutron scattering, in part due to a poor data collection rate and a difficult procedure for quantitative data analysis. Neutron scattering has remained the main vehicle for determining phonon dispersion curves as it offers both energy and momentum resolution well matched to materials studies, at the cost of a long data acquisition time, large required minimum sample volume, and a technically demanding experiment as compared to the TDS method.^{2,3}

The situation has changed recently due to advances in synchrotron radiation instrumentation. Undulator beams at third-generation synchrotrons, such as the Advanced Photon Source, now yield a brightness many orders of magnitude higher than a conventional laboratory source. This improvement in photon flux combined with modern computational capabilities has made it possible to carry out detailed quantitative phonon studies via x-ray TDS measurements as demonstrated in recent work on Si.^{4,5} The method is appealing for several reasons: (1) x rays can be focused down to sub-micron or even smaller spots, thus allowing investigations of very small crystals; (2) the method is highly efficient, and high-quality data can be collected within seconds; and (3) the deep penetrating power of x rays allows *in situ* studies under various environments. However, Si is one of the most perfect crystalline materials available, and questions have arisen as to whether or not the TDS method can be applied, with comparable accuracy, to other “more common” materials with significant structural defects that can affect such analysis. To address this issue, we have chosen to investigate Nb as a test case.

The choice of Nb is also motivated by a long history of interest in the lattice dynamics of this material.^{6–10} Its phonon dispersion exhibits a number of pronounced anomalies caused by a strong electron-phonon interaction involving long-range forces. This strong interaction is the underlying reason for the unusually high superconducting transition temperature compared to all other elements in the periodic table. The phonon anomalies have attracted much theoretical

interest, and attempts have been made to relate these to the 4*d* electronic structure of Nb.¹¹ These issues have also spurred the neutron scattering community to carry out detailed measurements of the phonon dispersion curves,^{6–10} which are thus available for comparison with our TDS results. As shown below, our TDS measurements yield phonon dispersion curves that are very close to the neutron results. The agreement, however, is not quite as good as in the case of Si, and the reasons for this difference will be discussed.

We should add that inelastic x-ray scattering has also become a competitive method for phonon measurements.¹² This method, like neutron scattering, has the advantage of energy resolution and is capable of direct mapping of the dispersion curves. However, the required instrumentation is much more complex, and the measurement is generally limited to one point in *k* space at a time. So far, only a limited number of systems have been examined by this method, and Nb is not one of these.

Our experiment was performed at the undulator beamline of UNICAT (University, Industry, and National Laboratory Collaborative Access Team) at the Advanced Photon Source, Argonne National Laboratory. A transmission Laue geometry was employed, in which an 18.7-keV beam was sent through a crystalline Nb foil of thickness 0.1 mm. The foil crystal was prepared by prolonged vacuum annealing of a high-purity polycrystalline foil, resulting in recrystallization over much of the area to form a single crystal oriented with the [110] direction normal to the foil surface. A charge-coupled device (CCD) was used as an area detector, positioned behind the sample to record the transmission scattering images with an exposure time of 5 s each. The incident beam was polarized in the horizontal direction. Data were taken with the sample in air.

Figures 1(a)–1(c) are experimental images of Nb which are, respectively, taken at near normal incidence to the crystal, with the crystal rotated 20° about an arbitrary axis and with the crystal rotated 40° about the same axis. The total data acquisition time for the entire experiment is about 15 s. These images are displayed on a logarithmic intensity scale in order to bring out weak features that are otherwise not visible to the eye. Figures 1(d)–1(f) are the corresponding theoretical images to be discussed below. The intensity pat-

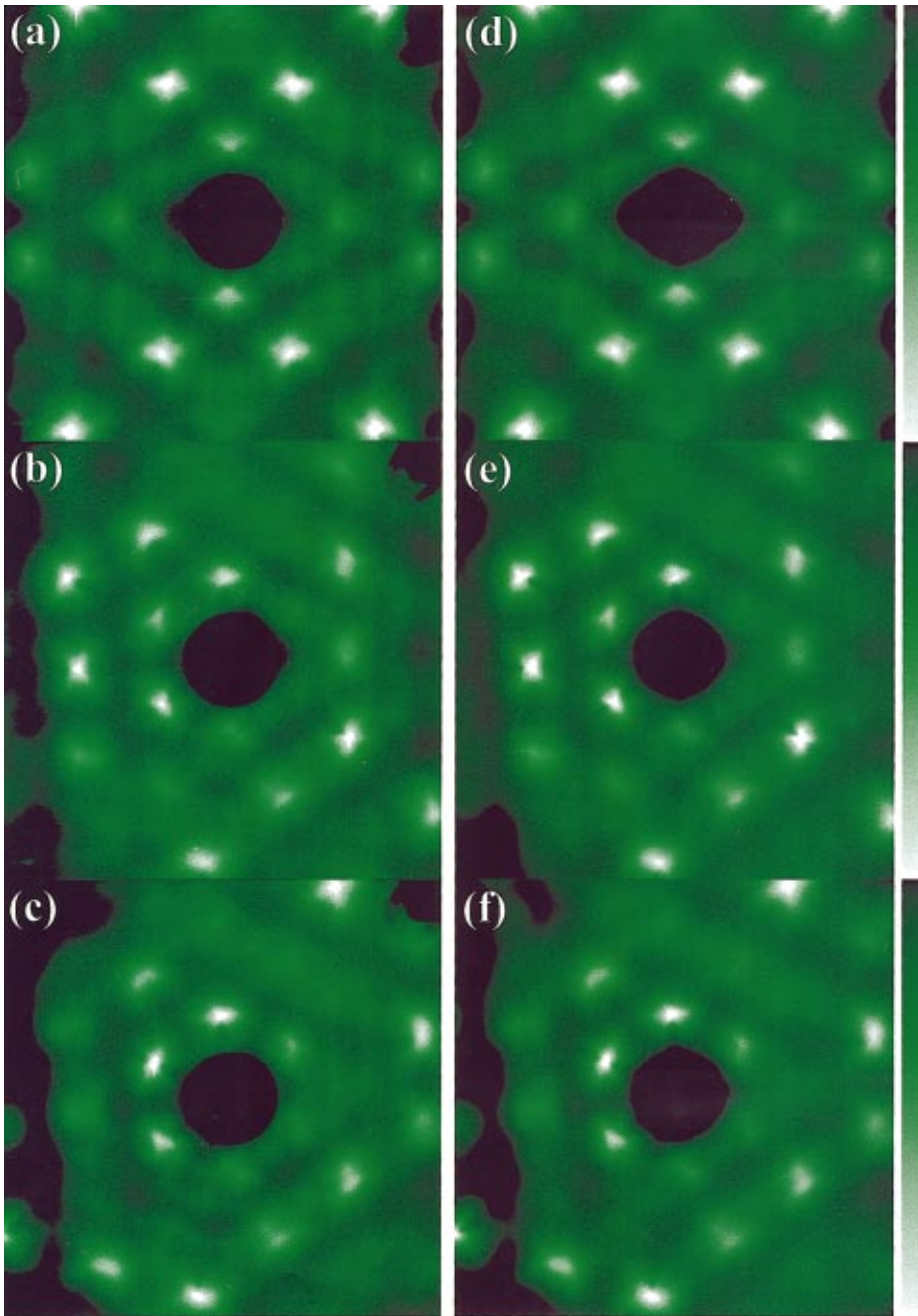


FIG. 1. (Color) Transmission x-ray scattering images taken from Nb(110) (a) at near normal incidence, (b) with the sample rotated 20° about an arbitrary axis, and (c) with the sample rotated 40° about the same axis. In each case, the shadows of a beam stop in the center of the image and a suspension post in the upper right-hand corner are evident. The corresponding calculated images based on a best simultaneous fit are shown in (d)–(f).

tern in each case is due to x-ray scattering from thermally populated phonons. Figure 1(a) exhibits a twofold rotational symmetry and reflection symmetries about the horizontal and vertical axes, while the other two patterns reveal no apparent symmetries due to the arbitrary rotations. By virtue of the wavelength selected, the Bragg condition is never satisfied over the entire area of detection in each case. Thus none of the bright spots are caused by crystal diffraction. The circular shadow of a suspended beam stop is visible at the center of each experimental image, and a shadow due to a suspension post is in the upper right corner.

Each point in a TDS picture corresponds to a unique momentum transfer \mathbf{q} determined by the scattering geometry and the x-ray wavelength employed in the experiment. In the case of Nb with just one atom per unit cell there are three

phonon modes at each \mathbf{q} contributing to the scattering intensity. The bright spots in each picture are points on the Ewald sphere that are closest to neighboring reciprocal lattice points, where the acoustic phonon population is high, leading to a high scattering rate. Due to the close proximity of the detector to the sample, a large scattering angle is achieved at the edge of each picture. The maximum momentum transfer is 8 \AA^{-1} in our experiment, which is significantly larger than the Brillouin zone size of Nb (the distance between the zone center and the H point on the zone edge is only 1.9 \AA^{-1}). Pictures taken at different sample rotation angles correspond to the same Ewald sphere intersecting the crystal Brillouin zones at different angles. Thus the three pictures in Fig. 1 together yield a substantial sampling of the reciprocal space.

The theoretical pictures shown in Figs. 1(d)–1(f) are de-

rived from a force constant formalism of lattice dynamics also known as the Born–von Karman model as described in standard textbooks. Force constants up to the eighth nearest neighbors are included in a harmonic lattice model, and diagonalizing this dynamic matrix results in phonon eigenmodes over the entire Brillouin zone. The intensity of scattering by an unpolarized incident x ray at a certain momentum transfer \mathbf{q} is given by a sum over the contributions from the three phonon branches:¹³

$$I_0 \propto f^2 e^{-2M(\mathbf{q})} \sum_{j=1}^3 \frac{|\mathbf{q} \cdot \hat{\mathbf{e}}_j(\mathbf{q})|^2}{\omega_j(\mathbf{q})} \coth\left(\frac{\hbar \omega_j(\mathbf{q})}{2k_B T}\right). \quad (1)$$

In this equation, f is the atomic scattering factor taken from standard x-ray tables, M is the Debye–Waller factor calculated using the same force constant model, ω is the phonon frequency, $\hat{\mathbf{e}}$ is the polarization vector of the phonon mode, k_B is the Boltzmann constant, T is the sample temperature (300 K), and j is the index for the three acoustic phonon branches. The hyperbolic cotangent function in this equation represents a sum of the Bose–Einstein distribution function and the zero-point mode occupancy.

The calculated intensity in each pixel, on a logarithmic scale, is given by

$$I_{\text{theory}} = \ln(\cos^3(2\theta)T(\theta, \phi) \{[\sin^2 \phi + \cos^2 \phi \cos^2(2\theta)] \times (AI_0 + B) + C(\theta)\} + D). \quad (2)$$

In this equation, ϕ is the azimuthal angle between the plane of polarization of the incident beam and the scattering plane, and 2θ is the scattering angle. The expression within the brackets containing these angles accounts for the linear polarization of the incident beam. The quantity A is an intensity normalization factor, B represents a constant background from higher order and defect scattering from the sample, C represents a slowly varying sample generated background including the tabulated Compton scattering for Nb (interpolated at each pixel) plus sample fluorescence represented by a Lorentzian, and D is an overall constant background related to the detector noise and response. The sample attenuation, given by $T(\theta, \phi)$, is calculated using the distances traveled by the incident and scattered beams for the particular sample orientation. One factor of $\cos(2\theta)$ on the left-hand side of the formula is for solid angle conversion associated with planar projection, and the additional $\cos^2(2\theta)$ factor allows for the inverse square distance dependence of the scattering intensity from the sample to different points on the detector plane.

Equations (1) and (2) are used to generate theoretical images, and these are used in a least-squares, pixel-by-pixel fit to all three experimental images simultaneously. The areas in the images around the beam stop and the support post in the upper right-hand corner were removed from the fit via a mask function. The fitting parameters include A , B , C , and D above, the three Euler angles determining the sample orientation, the exact distance from the sample to the CCD screen,

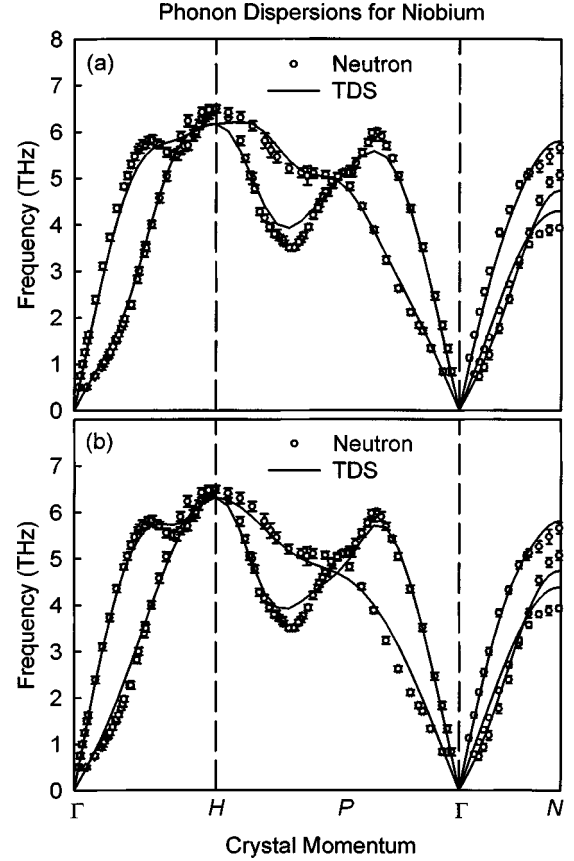


FIG. 2. Phonon dispersion curves of Nb. Open circles with error bars are neutron scattering data from Ref. 10. Solid curves are derived from a best fit to the TDS patterns based on a lattice dynamic calculation using (a) an eighth-nearest-neighbor Born–von Karman model and (b) a third-nearest-neighbor Born–von Karman model modified to account for charge fluctuations.

the x and y positions of the screen relative to the beam, and the Born–von Karman force constants.

The fitting of calculated images to the data can essentially be thought of as numerically solving Eq. (1) to reproduce the phonon frequencies as a function of momentum transfer. The images from the best fit are shown in Fig. 1. These are very close to the corresponding experimental images. The detailed shapes of the bright spots, some of which exhibit a “star” pattern, as well as the subtle variations of the less intense, diffuse regions are all well reproduced. There are differences on a small subset of pixels, however, such as the faint streaks in the experimental pictures extending from the brightest spots upward to the edge of each picture. This is particularly noticeable for the bright spot on the left in Fig. 1(c). These streaks are not seen in the calculation and are caused by the nonideal behavior of the charge-coupled device. In most applications, this streaking is not noticeable. In the present case, the use of a logarithmic intensity scale to bring out weak features accentuates the problem. While this does not spoil the picture in any major way, the “noise” introduced can potentially affect the accuracy of the fitting parameters.

The phonon dispersions along high-symmetry directions obtained from the best fit are shown in Fig. 2(a) by the solid

curves. These compare fairly well with the circles which represent results deduced from neutron scattering. The agreement is very good at low frequencies, but at high frequencies, there are noticeable differences in certain regions in the Brillouin zone, with the maximum deviation up to about 10%. The overall fit is certainly not quite as good as in the case of Si previously reported.⁵ This might be due to a confluence of several factors that affect the analysis. First, due to the anomalies in the dispersion, very-long-range forces are needed to obtain a reasonable description of the phonon dispersion curves.^{6–10} It is known that even the eighth-nearest-neighbor Born–von Karman model cannot reproduce all the features seen in the neutron data when fit directly. Thus some discrepancies are expected. Second, it has been suspected that the shortfall of the force constant model might get worse as one moves away from the high-symmetry directions probed in the neutron studies. Since the bulk of our TDS data are taken from regions in the reciprocal space off the high-symmetry directions, the limitations of the model can be exacerbated when the comparison is made only along high-symmetry directions. Third, the disagreement is mostly in the high-frequency regions, where TDS intensity is the lowest and noise on a logarithmic scale becomes correspondingly more important. The streaking problem mentioned above may very well have contributed to this disagreement. It is noted that Chang and Colella have reported some systemic discrepancies between x-ray and neutron results for the lattice dynamics of Nb.¹⁴ However, this might have been caused by variations in sample quality as discussed by Rowe and Magerl.¹⁵ We believe that our sample, grown in vacuum at high temperatures, is free from the impurities that might have significantly affected the earlier x-ray measurements.

Fitting of the images using the Born–von Karman model was a rather demanding computational job due to the large number of pixels that need to be calculated and the large number of force constants that need to be optimized. Simpler models exist, but many of these yield relatively poor descriptions of the dispersion curves.⁶ A very promising model is the charge fluctuation model that involves many fewer parameters at the expense of a slightly worse description of the phonon dispersion curves.¹⁶ This model is based on a third-nearest-neighbor Born–von Karman model, with the important modification that the ionic charges on the atoms are allowed to redistribute. This model is also employed in our analysis, and the resulting dispersion curves are shown in Fig. 2(b). The computation time is very much reduced, but a main drawback of this model is that it cannot reproduce sev-

eral observed features such as the “swoop” anomaly in the lowest transverse acoustic branch dispersion near the Γ point [specifically, compare Figs. 2(a) and 2(b) near Γ along Γ - H ; the dispersion goes up linearly from Γ and then drops below the linear extrapolation]. As a result, the fit in the low-frequency regions is compromised, while the discrepancies in the high-frequency regions remain. This example illustrates that the TDS method, as implemented here, is limited by the model used for fitting. A poor model can lead to significant errors in the result.

In summary, the present work offers a test of the TDS method with fairly satisfactory results on a system that has been the subject of intensive studies of its lattice dynamics. The “swoop” anomaly that is the focus of numerous previous studies is accurately reproduced. The crystalline quality of our Nb foil sample cannot be compared with that of the Si wafers used in previous studies, but the slightly worse fit here is unlikely to be sample related. Rather, the limitations of the force constant model and the imperfections of the charge-coupled device as a detector appear to be the main issues. None of these is fundamental in nature and can be overcome as the methods become further refined. A significant advantage of the TDS method is its efficiency, as the entire data acquisition time for this experiment is just 15 s and the data cover a very wide range in the reciprocal space. No special efforts were required in aligning and orienting the sample. This work thus illustrates both the powers and the limitations of the TDS method for materials studies.

This work was supported by the U.S. Department of Energy (Division of Materials Sciences, Office of Basic Energy Sciences) under Grant No. DEFG02-91ER45439. The UNICAT facility at the Advanced Photon Source (APS) is supported by the University of Illinois Frederick Seitz Materials Research Laboratory (U.S. Department of Energy and the State of Illinois-IBHE-HECA), the Oak Ridge National Laboratory (U.S. Department of Energy under contract with Lockheed Martin Energy Research), the National Institute of Standards and Technology (U.S. Department of Commerce), and UOP LLC. The APS is supported by the U.S. Department of Energy, Office of Science, under Contract No. W-31-109-ENG-38. Acknowledgments are also made to the Donors of the Petroleum Research Fund, administered by the American Chemical Society, and to the National Science Foundation Grant No. DMR-0203003 (T.C.C.) for partial support in connection with the synchrotron beamline operation.

*Email address: t-chiang@uiuc.edu

¹J. Laval, C. R. Hebd. Seances Acad. Sci. **207**, 169 (1938).

²G. Dolling, *Inelastic Scattering of Neutrons in Solids and Liquids* (IAEA, Vienna, 1963).

³Y. Nakagawa and A. D. B. Woods, *Lattice Dynamics* (Pergamon, Oxford, 1969), p. 39.

⁴Z. Wu *et al.*, Phys. Rev. B **59**, 3283 (1999).

⁵M. Holt *et al.*, Phys. Rev. Lett. **83**, 3317 (1999); M. Y. Chou and M. Choi, *ibid.* **84**, 3733 (2000); M. Holt and T.-C. Chiang, *ibid.* **84**, 3734 (2000).

⁶P. H. Dederichs and H. Schober, in *Metals: Phonon States, Electron States and Fermi Surfaces*, edited by K.-H. Hellwege and J. L. Olsen, Landolt-Börnstein, New Series, Group III, Vol. 13, pt. a (Springer-Verlag, Berlin, 1981), p. 96. This article contains a detailed listing of references and a review of the lattice dynamics models and the neutron scattering results.

⁷Y. Nakagawa and A. D. B. Woods, Phys. Rev. Lett. **11**, 271 (1963).

⁸R. I. Sharp, J. Phys. C **2**, 421 (1969).

⁹B. M. Powell, A. D. Woods, and P. Martel, *Neutron Inelastic*

- Scattering* (IAEA Vienna, 1972), Vol. 43.
- ¹⁰F. Guthoff, B. Hennion, C. Herzig, W. Petry, H. R. Schober, and J. Trampenau, *J. Phys.: Condens. Matter* **6**, 6211 (1994).
- ¹¹K.-M. Ho, C.-L. Fu, and B. N. Harmon, *Phys. Rev. B* **28**, 6687 (1983); **29**, 1575 (1983).
- ¹²See, for example, F. Occelli, M. Krisch, P. Loubeyre, F. Sette, R. Le Toullec, C. Masciovecchio, and J.-P. Rueff, *Phys. Rev. B* **63**, 224306 (2001).
- ¹³B. E. Warren, *X-Ray Diffraction* (Dover, New York, 1969).
- ¹⁴S. S. Chang and R. Colella, *Phys. Rev. B* **15**, 1738 (1977).
- ¹⁵J. M. Rowe and A. Magerl, *Phys. Rev. B* **21**, 1706 (1980).
- ¹⁶N. Wakabayashi, *Solid State Commun.* **23**, 737 (1977).